

# Adsorption artificial tree for atmospheric carbon dioxide capture, purification and compression



# Adsorption artificial tree for atmospheric carbon dioxide capture, purification and compression

*Giulio Santori* * [a], *Charithea Charalambous* [a], *Maria-Chiara Ferrari* [a], *Stefano Brandani* [a]

[a]The University of Edinburgh, School of Engineering, Institute for Materials and Processes, Sanderson Building, The King's Buildings, Mayfield Road, EH9 3FB, Edinburgh, Scotland, UK.

*__Corresponding author__:
Dr. *Giulio Santori*, Senior Lecturer,
The University of Edinburgh, The King's Buildings,
School of Engineering, Sanderson Building,
Institute for Materials and Processes,
Edinburgh, EH9 3BF

Tel. +44 (0)131 651 9043
Fax +44 (0)131 650 6551

# Adsorption artificial tree for atmospheric carbon dioxide capture, purification and compression


## Abstract

The current concentration of carbon dioxide in the atmosphere demands for development of negative emission solutions such as direct carbon dioxide removal from the atmosphere (air capture). Many well-established processes can remove carbon dioxide from the atmosphere but the real technological challenge consists of concentrating and compressing carbon dioxide at the conditions for long term geological storage, with efficient use of non-fossil energy sources. A thermally-driven, negative-carbon adsorption process for capture, purification and compression of carbon dioxide from air is proposed. The process is based on a series of batch adsorption compressors of decreasing size to deliver a compressed carbon dioxide stream to a final storage. Thermodynamic analysis of the process shows that, by exploiting the equilibrium properties of commercial and non-commercial materials, carbon dioxide can be produced at specifications appropriate for geological storage. By operating the process with zeolite 13X at regeneration temperature of 95°C, a final storage vessel can be pressurized with carbon dioxide at purities >0.95 mole fraction and specific energy consumption <2.2 $MJ_{th}$ $mol_{CO2}^{-1}$. Tailored materials provide a step-change in performance. When the process operates with zeolite NaETS-4, carbon dioxide can be purified at values >0.97 mole fraction.


## 1. Introduction

Atmospheric $CO_2$ concentration is approaching 450 ppm by 2035, resulting in a 77–99% probability of exceeding 2°C global warming [1] with consequent dramatic economy damage [2]. The initial plans for emissions reduction were based on a combination of increased use of renewable energy and carbon dioxide capture from industrial sources and power plants, including steps of transport and storage into geological formations [3]. The steady acceleration of the average global $CO_2$ concentration in the atmosphere demonstrates that such plans have not been put into action and negative emission solutions which could be disregarded decades ago, have to be considered now.

Direct air capture (DAC) enables $CO_2$ removal from ambient air [4, 5]. DAC is an option mentioned by the last assessment reports of the Intergovernmental Panel on Climate Change [6] as a measure to address directly the cause of climate change. In order to have reasonable effect on global warming, DAC technologies have to be deployed on a scale directly linked to the global petroleum consumption, which totalled 4.3 Gt in 2016 [7]. Accordingly, DAC technologies have to capture $CO_2$ on a scale of at least the same order of magnitude per year, at performance higher than the natural mechanisms of $CO_2$ capture from the atmosphere such as trees.

Table 1: comparison of performance between trees and two different air capture energy consumption prediction.

| | Solar Energy [MJ $m^{-2}$ $day^{-1}$] | Capture rate [$t_C$ $ha^{-1}$ $yr^{-1}$] | Recovery | Purity [mole fraction] | Specific energy [MJ $kg_{CO2}^{-1}$] | Surface area for 1Gtonne $CO_2$ capture [$km^2$] | Function | Ref |
|---|---|---|---|---|---|---|---|---|
| Tree (Fagus Sylvatica) | 9.4-16.2[a] | 4.9 | -- | -- | 7000-12000 | 2041000 | Capture & utilization | [8] |
| Thermodynamics (value function) | 4.7-8.1[b] | 350-210 | 0.5-0.98 | 0.95 | 49-141 | 28600-47700 | Capture & purification | [11-13] |
| Thermodynamics (Gibbs energy of mixing) | 4.7-8.1[b] | 38500-61500 | 0.5-0.98 | 0.95 | 0.44-0.48 | 160-260 | Capture & purification | |

Note:
[a] one of the tree species having highest $CO_2$ capture rate is Fagus Sylvatica with 4.9 $t_C$ $ha^{-1}$ $yr^{-1}$ [8]. This species grows throughout Europe, where the annual average daily global solar radiation on the horizontal plane ranges 9.4-16.2 MJ $day^{-1}$ $m^{-2}$ [14].
[b] solar energy collection efficiency is assumed 50% [15].

Table 1 shows a performance comparison between the tree species having highest capture rate and the values derived from thermodynamic considerations. The adoption of trees would require the allocation of a surface area too high to be feasible and considerations based on the ideal free energy of mixing [9] are too optimistic to be reliable since no practical process exists separating extremely dilute mixtures and consuming an amount of energy proximal to the ideal free energy of mixing [10]. Assessments based on the value function [11, 12] reveal the intrinsic energy intensity of DAC technologies. Moreover, it is essential to use renewable primary energy to power an air capture process, because it would be futile if $CO_2$ was captured using energy that, as a net effect, produces $CO_2$ [13]. Among all the renewable energy primary sources, the only one that can deal with the DAC scale of deployment is solar energy [16], although the utilization of other renewable energy sources is still possible at smaller scales. Accordingly, DAC needs of large installation surface areas used mainly to allocate the devices for primary energy collection. Therefore, every constraint to the installation surface area of the collection systems is going to impact directly on the maximal capture rate achievable.

Furthermore, higher costs and energy penalties are expected for the first scale-up attempts as usually happens for low readiness level technologies even when the scale-up factor is limited to 3-15 orders of magnitude [17, 18]. Moreover, as highlighted elsewhere [19] the capture, compression and purification sites have to be located at reasonable distance from the storage sites. All these aspects suggest that DAC alone is not a viable solution to reverse the trend of $CO_2$ concentration in the atmosphere while emissions continue to be at the current rate. Only point-source carbon capture and the implementation of renewable energy generation systems have the right potential to stabilise the current trend of atmospheric $CO_2$ concentration. After stabilisation, the role of DAC technologies is to restore the atmospheric carbon to the natural equilibrium values, by cooperating with the natural mechanisms of carbon capture which otherwise would require centuries [8]. Hence, air capture is a measure that can be used for $CO_2$ which has not been captured at the source and this includes the carbon already emitted for centuries. Accordingly, the proposition "point-source carbon capture" vs. "air capture" that often populates the open scientific literature [20, 21] is inappropriate because discourages both the research areas which nowadays are unavoidable. The only removal of $CO_2$ at extremely dilute conditions has been already shown elsewhere as being viable for many adsorption materials [22-26]. $CO_2$ removal technologies such as the air revitalization system in the International Space Station [27] or $CO_2$ separation in commercial cryogenic air separation units [28] have worked for years. The real technological challenge is not to separate $CO_2$ from air but concentrate and compress that amount of $CO_2$ at the specifications dictated by long term geological storage [13]. Table 2 summarizes the requirements that a DAC technology should fulfil to cope with a pipeline serving a geological storage site.

Table 2: $CO_2$ and process performance specifications for air capture

| Feature | Requirement | Note | Ref |
|---|---|---|---|
| Capture rate | >49 $t_{CO2}$ $ha^{-1}$ $yr^{-1}$ | 10 times the average value of the tree species having highest capture rate (Fagus Sylvatica). | [8] |
| Specific energy demand* | <50 MJ $kg_{CO2}^{-1}$ (<2.2 MJ $mol_{CO2}^{-1}$) | 2 orders of magnitude the free energy of mixing for an air capture system separating with 50% recovery. | |
| Purity | >95% | Impurities: $y_{H2O} < 0.05\%$; $y_{N2}+y_{O2}+y_{Ar} < 4\%$ These levels are set to contain the energy required for compression and to maintain high geological storage density. | [29, 30] |
| Pressure | >supercritical | 73.8 bar for pure $CO_2$ | [31, 32] |

Note: * the value results from value function calculation [11, 12]

Large scale DAC solutions were first proposed by Lackner [33] and Keith [34]. The initial approach to air capture was based on the use of aqueous solutions of NaOH, which spontaneously react with the dilute $CO_2$ of ambient air and high-purity $CO_2$ is achieved by means of oxy-fuel combustion of natural gas [35-38]. Mass and material balance calculation have shown that this process can be carbon net-negative [35] but an approach that uses fossil fuel, very high temperatures (oxy-combustion kilns) and corrosive solutions of NaOH is likely to have high costs. This led to propose a different approach based on moisture swing adsorption [39, 40]. This solution provides a maximum $CO_2$ purity ranging between 0.02-0.05 mole fraction at ambient pressure [41, 42], well below the specifications of Table 2. Moreover, the purification section of this system is undefined, and the requirements to dry the adsorbent entail regions of low humidity, unless regeneration is performed with an additional temperature-swing [42]. The final stream produced is atmospheric and has high water content mismatching again the specifications of Table 2. Similar issues concern a proposed steam swing adsorption systems for air capture [43]. The performance of a bubbling fluidized bed reactor using mesoporous polyethyleneimine–silica adsorbent has been evaluated elsewhere [44]. In this system the maximum $CO_2$ purity achieved is well below the limits suitable for geological storage and regeneration temperatures of 130°C points to concentrated solar thermal technologies which are more expensive and less efficient then solar flat plates [45]. More importantly, the energy required to flow high amounts of atmospheric air through fluidized bed reactors is higher than in other solutions (e.g. monoliths), being the pressure drops across this type of reactor higher. Traditional vacuum and temperature swing adsorption could be also used for DAC [46, 47], but the use of high vacuum pumps relies on components requiring significant power, maintenance and low scalability [48]. In these systems, pressure of the output stream is ambient and water is often part of the stream components. These features make the output stream inadequate to the most common solutions for long term geological storage [49]. Further to engineering considerations, the optimal size of each individual technology unit also depends on a set of interrelated economic and social factors [50, 51] which are unpredictable so far. The current scenario shows that there is no viable device for global-scale DAC yet and, if in few decades the international targets have to be achieved [52], further efforts have to be devoted to engineering systems which

can address the limitations described above. Aligned with this need, a process for DAC based on a sequence of adsorption beds powered by heat at 95°C is formulated. The present temperature swing adsorption process has the distinct feature to use heat not only to remove $CO_2$ from the atmosphere but also to purify and compress it. Furthermore, this process can be powered only with heat, therefore without the need of moving components such as vacuum pumps which is characteristic of other temperature swing adsorption systems where high-vacuum is essential to achieve high $CO_2$ purity. Nevertheless, the optional application of a moderate level of vacuum also to the proposed process, can enhance its performance. The utilization of adsorption materials facilitates the process scalability. As already demonstrated in other fields [53, 54], adsorption processes can be easily scaled-up mainly by increasing the amount of material used. Finally, the following analysis is applicable across different technological scales since the results are specific to the amount of captured $CO_2$. In the analysis that follows the process thermodynamics is challenged against the thresholds in Table 2.

**2. Description of the process**

In Fig. 1 a simplified but comprehensive overview of the system is depicted. The system is composed by one adsorption bed (Bed 1) for $CO_2$ removal from air, a series of adsorption beds for compression and purification (Bed 2, Bed 3,… Bed NB) and one final bed (storage bed) which will store purified $CO_2$ and work as a buffer to an eventual $CO_2$ pipeline. Once full, the storage bed can be heated to discharge $CO_2$ directly into the pipeline. In order to work optimally, the structural features required to each bed have to be different. Bed 1 has to process high flow rates of air, therefore its pressure drops have to be minimal in order to contain the power needed for air flowing. This points to laminate type of beds [55, 56] or parallel passage contactors [57, 58]. Conversely, the storage bed and all the compression beds from 2 to NB must have high density, in order to minimize voids and store increasingly high amounts of $CO_2$.

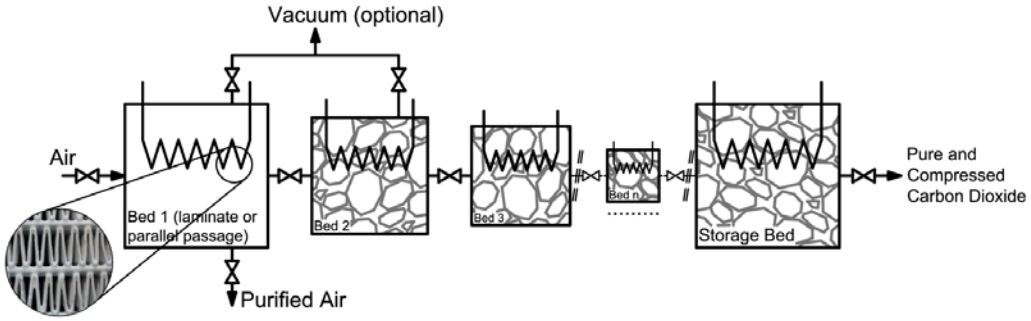


Figure 1: Block diagram of the temperature swing adsorption process to capture, compress and purify carbon dioxide from atmospheric air

The system is operated according to the procedure described in Table 3 which, as exemplification, is referred to a 5 beds process (Bed 1: adsorption bed, Beds 2 to 4: compression and purification beds and Bed 5: storage bed). Atmospheric air flows through the first bed where $CO_2$ is adsorbed along with other less strongly adsorbed compounds. By heating Bed 1, a $CO_2$-rich stream is desorbed to the next connected bed (Bed 2), which is cooled. This heating/cooling process is repeated for two times (Bed 2-Bed 3 connection, Bed 3-Bed 4 connection) to pour an increasingly pure stream to Bed 4. Finally, by using the same heating-cooling process, an amount of purified $CO_2$ is stored in the last bed (Bed 5: storage bed) from Bed 4. As already observed and extensively explained elsewhere [59-61], an additional benefit from this process is the significant pressure increase along the beds train until reaching a maximum in the storage bed. The procedure listed in Table 3 is repeated from Bed 1 to Bed 5 several times (runs) until the $CO_2$ concentration in Bed 5 reaches a stable value. Thus, in run 2 atmospheric air flows again through Bed 1 (step 1) that is then purged (optional, step 2), isolated and heated (step 3) while Bed 2 is cooled (step 3). Bed 1 and Bed 2 are connected again (step 4). Bed 2 is quickly purged (optional, step 5), then isolated and heated (step 6) while Bed 3 is cooled (step 6). The steps follow in the same way described above and reported in Table 3. An important feature of the process is that run after run Bed 1 returns at the same initial condition while in all the other beds, $CO_2$ concentration and individual bed pressure build up because of the residual amount of gas from the previous run.

The process is intermittent, since Bed 5 is fed only at the end of each run, and can either be operated following the natural day/night cycle or at higher frequency by assembling more than one queue of beds to fill one common storage bed. In this last case the process would require additional thermal storages and heating/cooling loops to manage the temperature swings. One final compression takes place in the end of all runs by isolating and heating the storage bed. After compression, the storage bed blowdown can deliver pure and compressed $CO_2$ to the pipeline at variable flowrate and pressure.

A preliminary regeneration procedure is operated before the steps of Table 3. This procedure is aimed to prepare the system by minimising the amount of unwanted gases consisting mainly of $N_2$. The procedure includes an initial heating for all the beds, then a blowdown [62] down to mild vacuum pressure (i.e. >30 kPa, achievable with ejectors and easily scalable), isolation of each single bed and cooling at constant volume. In this way, the operation starts with all the beds at pressure lower than ambient and minimal residual gas content. Vacuum can be also applied before Bed 1-Bed 2 equilibration (step 2 in Table 3) and before Bed 2- Bed 3 equilibration (step 5 in Table 3) to purge the system of $N_2$, enhancing therefore the performance of the process. The mild level of vacuum needed is easily achievable by means of simple liquid jet ejectors, making the whole process almost free from moving components.

Table 3: Process steps sequence with indication of the equilibrium temperatures

| Bed | Steps [a] | | | | | | | | | | |
|---|---|---|---|---|---|---|---|---|---|---|---|
| | 1 | 2 (opt) | 3 | 4 | 5 (opt) | 6 | 7 | 8 | 9 | 10 | 11 |
| 1 | A ($T_{low}$) | B ($T_{high}$) | H ($T_{high}$) | E 1/2 ($T_{high}$) | -- | -- | -- | -- | -- | -- | -- |
| 2 | -- | -- | C ($T_{low}$) | E 1/2 ($T_{low}$) | QV ($T_{low}$) | H ($T_{high}$) | E 2/3 ($T_{high}$) | -- | -- | -- | -- |
| 3 | -- | -- | -- | -- | -- | C ($T_{low}$) | E 2/3 ($T_{low}$) | H ($T_{high}$) | E 3/4 ($T_{high}$) | -- | -- |
| 4 | -- | -- | -- | -- | -- | -- | -- | C ($T_{low}$) | E 3/4 ($T_{low}$) | H ($T_{high}$) | E 4/5 ($T_{high}$) |
| 5 | -- | -- | -- | -- | -- | -- | -- | -- | -- | C ($T_{low}$) | E 4/5 ($T_{low}$) |

Note: [a] Nomenclature of the acronyms used to identify beds' states:
A: Adsorption. Air flows through Bed 1 at ambient temperature and pressure.
B: Blowdown. Optional vacuum step where Bed 1 is led to $P_{vacuum}$.
H: Heating. Bed is isolated and then heated up at constant volume.
C: Cooling. Bed is isolated and then cooled down at constant volume.
QV: Quick Vacuum. Optional step of quick vacuum at frozen adsorbed phase.
E *j*/*j+1*: Equilibration between Bed *j* and Bed *j+1*. Bed *j* is connected with Bed *j+1*. The two beds share the same bulk gas phase. Bed *j* is kept at $T_{high}$ and desorbs while Bed *j+1* is at $T_{low}$ and desorbs. This results in a $CO_2$ enrichment in Bed *j+1*.

## 3. Process thermodynamics

The approach neglects mass and heat transfer kinetics that would otherwise overshadow the maximal limiting performance of the process. These phenomena are important factors contributing to the practical process efficiency, nevertheless the analysis focuses on understanding whether or not the process can meet the performance required for air capture. The assumptions of this thermodynamic analysis are:

1) Each single bed is homogeneous in temperature and pressure;
2) The bulk gas phase and adsorbed phase of each single bed are two distinct homogeneous phases;
3) The fluid mixture is ideal in bulk gas phase and in adsorbed phase;
4) The difference in bulk gas phase concentration of two consecutive connected beds due to the different temperatures is negligible;
5) Air is a mixture of $N_2$, $O_2$ and $CO_2$.

The description of the mathematical model is restricted to the case of zeolite 13X adsorbent as benchmarking material, but the model can be easily extended to other adsorption materials. Air is assumed consisting of $N_2$, $O_2$, and $CO_2$, with all the remaining trace components included in the $N_2$ concentration. This assumption relies on the presence of a desiccant system upstream the process or insensitivity of the adsorption material to water adsorption at ambient conditions [63, 64]. Adsorption of $N_2$ and $O_2$ on zeolite 13X is described with Langmuir isotherm while $CO_2$ with Dual-Site Langmuir isotherm:

$$n_i = q_{s1,i}\frac{P_i\, b_{01,i} e^{\left(-\Delta H_{1,i}/RT\right)}}{1+P_i\, b_{01,i} e^{\left(-\Delta H_{1,i}/RT\right)}} + q_{s2,i}\frac{P_i\, b_{02,i} e^{\left(-\Delta H_{2,i}/RT\right)}}{1+P_i\, b_{02,i} e^{\left(-\Delta H_{2,i}/RT\right)}} \qquad \text{i=N}_2\text{; O}_2\text{; CO}_2\text{;} \qquad (1)$$

where $n_i$ [mol kg$^{-1}$] is the amount of pure gas *i* adsorbed per unit of mass of empty adsorbent, $P_i$ [kPa] is the equilibrium partial pressure of the component *i* in the bulk gas phase, T [K] is the equilibrium temperature, $(q_{s1,i}, q_{s2,i}, b_{01,i}, b_{02,i}, \Delta H_{1,i}, \Delta H_{2,i})$ is the vector of adsorption isotherm parameters reported in Table 4, specific to

the individual gas adsorbed ($N_2$, $O_2$, $CO_2$). The saturation capacities are thermodynamically consistent with the assumptions of the Langmuir model, i.e. equal for all molecules.

Table 4: Langmuir and Dual Site Langmuir parameters

| Zeolite | Gas | $q_{s1,i}$ [mol kg$^{-1}$] | $b_{01,i}$ [kPa$^{-1}$] | $\Delta H_{1,i}$ [kJ mol$^{-1}$] | $q_{s2,i}$ [mol kg$^{-1}$] | $b_{02,i}$ [kPa$^{-1}$] | $\Delta H_{2,i}$ [kJ mol$^{-1}$] | Data source |
|---|---|---|---|---|---|---|---|---|
| 13X | $N_2$ | 5.64 | $1.969\ 10^{-7}$ | −20.20 | 0 | -- | -- | measured* |
| | $O_2$ | 5.64 | $5.227\ 10^{-7}$ | −15.69 | 0 | -- | -- | [65] |
| | $CO_2$ | 2.20 | $2.231\ 10^{-6}$ | –32.98 | 3.44 | $2.172\ 10^{-7}$ | −30.81 | measured* |
| NaETS4 | $N_2$ | 3.50 | $4.402\ 10^{-7}$ | –18.01 | 0 | -- | -- | [66] |
| | $O_2$ | 3.50 | $2.774\ 10^{-8}$ | –23.30 | 0 | -- | -- | [66] |
| | $CO_2$ | 2.50 | $6.174\ 10^{-8}$ | –42.03 | 1.00 | $1.094\ 10^{-9}$ | −40.88 | [66] |

Note: *parameters regressed on UOP zeolite 13X. Equilibrium data measured in the Adsorption Laboratory of The University of Edinburgh (www.carboncapture.eng.ed.ac.uk).

The volume occupied by the bulk gas phase ($V_{void,i}$) is calculated by the mass of each bed $m_{ads,i}$ [kg] through:

$$V_{void,j} = \frac{m_{ads,j}}{\rho_{bed,j}}\left(\varepsilon_{b,j} + \left(1-\varepsilon_{b,j}\right)\varepsilon_p\right) \qquad \text{j=1,2,..NB} \qquad (2)$$

$$\rho_{bed,j} = \left(1-\varepsilon_{b,j}\right)\left(1-\varepsilon_p\right)\rho_{cr} \qquad \text{j=1,2,..NB} \qquad (3)$$

where $\varepsilon_{b,j}$ is the bed void fraction of the *jth* bed, $\varepsilon_p$ is the solid void fraction and $\rho_{bed,j}$ [kg m$^{-3}$] is the bed density and $\rho_{cr}$ is the crystal density of the adsorbent material.

Adsorption on zeolite 13X of the present gas mixture at the process operating conditions can be reasonably assumed to follow the ideal adsorption solution theory (IAST) [67, 68]. During adsorption, Bed 1 is operated at atmospheric conditions and the adsorption is calculated according to the conventional solution procedure for IAST [69-71], by imposing bulk gas phase pressure and composition. In the case of heating and cooling of the beds at fixed volume, an isochoric-isothermal flash calculation for adsorption is required. For each single bed, the pressure and compositions at equilibrium can be calculated by solving system of equations in Table 5.

Table 5: Set of equations for isothermal-isochoric flash calculation

| | | |
|---|---|---|
| $\sum_i \frac{z_i\left(\frac{P_i^0}{P_{bulk}}-1\right)}{1+\frac{G}{F}\left(\frac{P_i^0}{P_{bulk}}-1\right)} = 0$ | i=$N_2$; $O_2$; $CO_2$; | (4) |
| $x_i = \frac{z_i}{1+\frac{G}{F}\left(\frac{P_i^0}{P_{bulk}}-1\right)}$ | i=$N_2$; $O_2$; $CO_2$; | (5) |
| $G = \frac{P_{bulk}V_{void}}{RT}$ | | (6) |
| $y_i = x_i\frac{P_i^0}{P_{bulk}}$ | i=$N_2$; $O_2$; $CO_2$; | (7) |
| $\frac{m_{ads}}{M} = \sum_i\left(\frac{x_i}{n_i^0}\right)$ | i=$N_2$; $O_2$; $CO_2$; | (8) |
| $\psi_i = \int_0^{P_i^0} n_i d(ln\ P_i)$ | i=$N_2$; $O_2$; $CO_2$; | (9) |
| $\psi_i = \psi_{eq}$ | i=$N_2$; $O_2$; $CO_2$; | (10) |
| $F - (G + M) = 0$ | | (11) |

Note: $n_i$ [mol kg$^{-1}$] in eq. (9) is the adsorption isotherm; $n_i^0$ is the specific number of moles [mol kg$^{-1}$] calculated using surface pressure $P_i^0$ [kPa] in the adsorption isotherm. All the other variables are specified in the nomenclature.

The system of eqns (4-11) can be reduced to only two equations by substitution of variables, holding the final variables $P_{bulk}$ [kPa] and reduced grand potential $\psi_{eq}$ [mol kg$^{-1}$]. The reduced two equations system includes eq. (4) and eq. (11). For the case where two beds are connected, the problem is formulated similarly by imposing the same pressure and bulk gas phase composition, at different bed temperatures and by including the global mass balance for each single component. It is worth noticing that the thermal gradient in the gas phase common to two consecutive connected beds promotes $CO_2$ enrichment in the cold bed by means of Soret effect, but given the limited difference of temperature between the two beds this effect is negligible [72, 73].

The results from the previous system of equations are used for the calculation of the enthalpy of adsorption. In the case of an ideal multicomponent mixture, the enthalpy of adsorption for each bed, $\Delta H_{ads}$ [kJ] is [74]:

$$\Delta H_{ads} = m_{ads} \sum_i (n_i \Delta h_i^*) \qquad \text{i=N}_2\text{; O}_2\text{; CO}_2\text{;} \qquad (12)$$

Where $n_i$ is the amount adsorbed and $\Delta h_i^*$ is the pure component molar integral enthalpy of adsorption [kJ mol$^{-1}$] of the *ith* component of the mixture. $\Delta h_i^*$ for an ideal gas is:

$$\Delta h_i^* = \int_0^{n_i^0} \Delta \bar{h}_i^* dn_i \qquad \text{i=N}_2\text{; O}_2\text{; CO}_2\text{;} \qquad (13)$$

where $\Delta \bar{h}_i^*$ is the pure component differential enthalpy [kJ mol$^{-1}$], which is computed as:

$$\Delta \bar{h}_i^* = RT^2 \left(\frac{\partial ln(P)}{\partial T}\right)_{n_i^0} \qquad \text{i=N}_2\text{; O}_2\text{; CO}_2\text{;} \qquad (14)$$

The heat required to power the process is also sensible heat. Under the assumptions that the specific heats of the gases are constant in the operating range of temperatures and the specific heats in adsorbed and bulk gas phase are identical [75], the sensible heat for each single bed is:

$$\Delta H_{sens} = m_{ads} c_{p,ads} \left(T_{high} - T_{low}\right) + \left(T_{high} - T_{low}\right) \sum_i \left(n_{i,bulk} + n_{i,ads}\right) c_{p,i} \quad \text{i=N}_2\text{; O}_2\text{; CO}_2\text{;} \qquad (15)$$

where $c_{p,ads}$ is the specific heat capacity of the adsorbent [kJ kg$^{-1}$ K$^{-1}$], $c_{p,i}$ is the bulk gas phase specific heat capacity of the *ith* component of the mixture [kJ mol$^{-1}$ K$^{-1}$], $n_{i.bulk}$ is the number of moles of component *i* in the bulk gas phase [mol] and $n_{i,ads}$ is the number of moles of component *i* in the adsorbed phase [mol].
Finally, the process requires a minimal amount of electrical energy for vacuum in Bed 1 and Bed 2. This is calculated as adiabatic compression work:

$$W_{el} = \frac{1}{\eta} \frac{\gamma_{mix}}{\gamma_{mix}-1} n_{proc} R T_{vacuum} \left[1 - \left(\frac{P_{vacuum}}{P_{Amb}}\right)^{\frac{\gamma_{mix}}{\gamma_{mix}-1}}\right] \qquad (16)$$

$$\gamma_{mix} = \frac{\sum_i y_i c_{p,i}}{\sum_i y_i c_{v,i}} \qquad \text{i=N}_2\text{; O}_2\text{; CO}_2\text{;} \qquad (17)$$

where $W_{el}$ is the energy consumed for vacuum [kJ] in Bed 1 or Bed 2, $\eta$ is the vacuum system efficiency, $n_{proc}$ [mol] is the amount of fluid processed (considering only the extracted amount from ambient to vacuum pressure), $T_{vacuum}$ is the gas temperature at the inlet of the vacuum system, $P_{vacuum}$ and $P_{Amb}$ [kPa] are respectively the applied vacuum pressure and the ambient pressure. Detailed guidelines on the utilization of the equations and calculation aids are reported in the Support Material.

## 4. Material balance

All the operating parameters of the process are listed in Table 6. The system is operated including the optional purge steps for Bed 1 and Bed 2.

Table 6: Parameters of the process for the base case

| | Value | Unit | Ref |
|---|---|---|---|
| $\varepsilon_{b,1}$ | 0.50 | -- | [55] |
| $\varepsilon_{b,2/3/4/5}$ | 0.25 | -- | |
| $\varepsilon_p$ | 0.20 | | [76] |
| $\rho_{cr}$ | 1500 | kg $m^{-3}$ | [77] |
| | | | |
| $T_{low}$ | 20 | °C | |
| $T_{high}$ | 95 | °C | |
| $P_{vacuum}$ | 30 | kPa | |
| $\eta$ | 0.6 | | |
| | | | |
| $m_{1/5}$ ratio | 5.65 | $kg_{Bed\ 1}\ kg_{Bed\ 5}^{-1}$ | |
| $m_{2/5}$ ratio | 1.01 | $kg_{Bed\ 2}\ kg_{Bed\ 5}^{-1}$ | |
| $m_{3/5}$ ratio | 0.34 | $kg_{Bed\ 3}\ kg_{Bed\ 5}^{-1}$ | |
| $m_{4/5}$ ratio | 0.14 | $kg_{Bed\ 4}\ kg_{Bed\ 5}^{-1}$ | |
| | | | |
| $^{a}c_{p,CO2}$ | 38.51 | J $mol^{-1}$ $K^{-1}$ | [78] |
| $^{a}c_{p,N2}$ | 29.16 | J $mol^{-1}$ $K^{-1}$ | [78] |
| $^{a}c_{p,O2}$ | 29.60 | J $mol^{-1}$ $K^{-1}$ | [78] |
| $^{a}c_{p,ads}$ | 858.0 | J $kg^{-1}$ $K^{-1}$ | [79] |
| | | | |
| $y_{N2,air}$ | 0.7897 | -- | |
| $y_{O2,air}$ | 0.2099 | -- | |
| $y_{CO2,air}$ | 0.0004 | -- | |

Note: [a] average value in the range 20°C-95°C

Fig. 2 shows the trend of species concentrations and pressure in Bed 5 (storage bed) up to 20 runs. A maximal pressure of 9.5 bar is reached, with ($z_{CO2}$, $z_{N2}$, $z_{O2}$) of (0.957, 0.041, 0.001) global mole fraction which comply with the purity targets of Table 2. One remarkable property of this process is that compression and purification are obtained by using thermal energy carried at temperatures of 95°C, which is a temperature level technically achievable with solar thermal energy collection systems [15, 16].

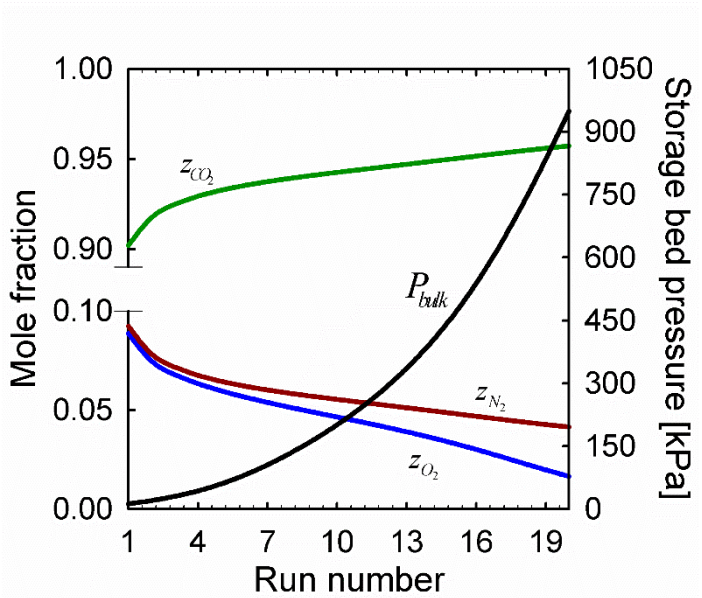


Figure 2: Pressure (black) and global mole fraction of $CO_2$ (green), $N_2$ (red) and $O_2$ (blue) in the storage bed (Bed 5).

Although 9.5 bar is still below the pressure target, $CO_2$ compression can be easily achieved by adjusting the adsorbent bed ratios and by heating the storage vessel, as investigated in detail elsewhere [60]. Fig. 3 shows

the maximal achievable pressure across a range of different heating temperatures assuming the compressed mixture as an ideal gas. This assumption is correct until ~20 bar but loses precision at higher pressures where $CO_2$ behaves non-ideally. Nevertheless, the trend reported in Fig. 3 is conservative because, as demonstrated in [60], the pressure achieved by heating a non-ideal adsorbed phase is higher than in the ideal case.

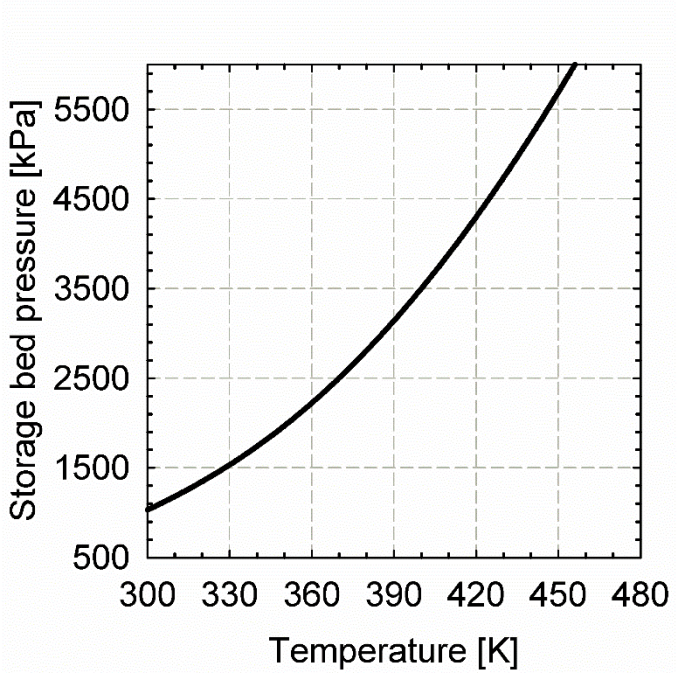


Figure 3: Pressure in the storage bed achieved by heating at constant volume.

Fig. 4 is illustrative of the material balance across the system after 20 runs. A total of 81 $m^3\,kg_{Bed\,1}^{-1}$ of air have to flow through Bed 1 and 99.7% of the inlet flow leaves the system as air, purified of $CO_2$ whereas 0.2% during the vacuum steps in Bed 1 and Bed 2. Captured $CO_2$ and co-adsorbed $N_2$ and $O_2$ are processed along the separation and compression beds. At run 20, a portion of process fluid is accumulated in Beds 1-4 and in Bed 5 that stores $CO_2$ at purities which are dependent on the mass ratios between beds.

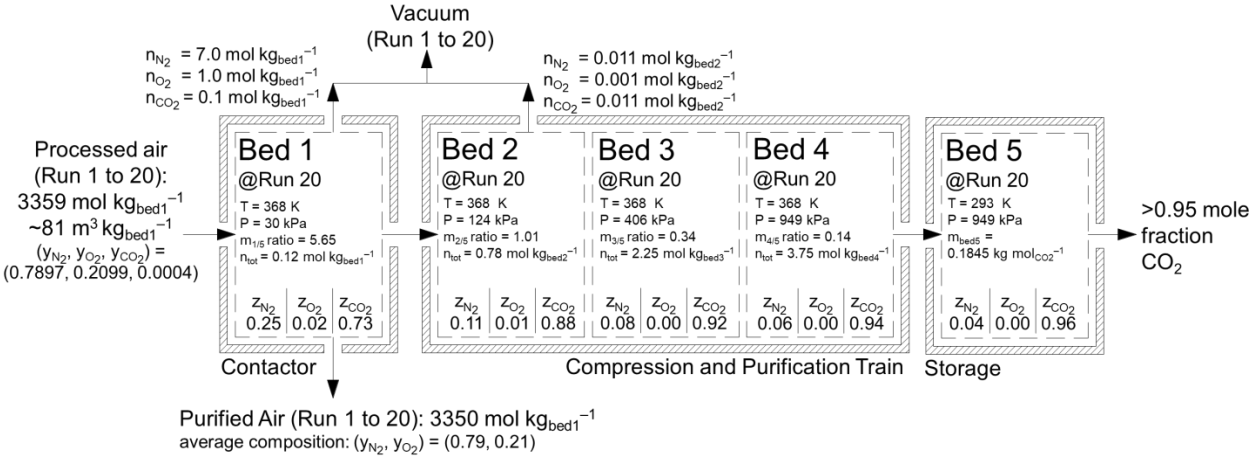


Figure 4: System material balance after 20 runs. $n_{tot}$ is the total amount of gas mixture in the bed, sum of the amount in bulk gas phase and adsorbed phase; $m_{i/5}$ is the mass ration between Bed *j* and Bed 5.

## 5. Energy balance

The process needs three different forms of energy that are heat at 95°C, cold at 20°C and electricity for the optional vacuum steps in Bed 1 and Bed 2. The temperature level required for cooling makes the ambient air suitable as cold utility while the hot utility supplies sensible heat and heat of desorption at temperatures compatible with flat plate solar thermal collector. Furthermore, the optional amount of electricity needed for vacuum can be also supplied with renewable sources. Therefore, there is no point in the process where $CO_2$ is generated. This features make the process completely carbon-negative.

Fig. 5 shows the trend of adsorption and desorption thermal energy needed to operate the system from run 1 to 20, highlighting the contribution of each state change:

-Bed 1: the bed is cooled during adsorption to keep it isothermal. This amount of energy is identical to the sum of the energy contributions for heating, blowdown and equilibration. The main heat duty is during equilibration when the gas stream has to be discharged from Bed 1 (desorbing) and Bed 2 (adsorbing).

-Bed 2, 3 and 4: the amounts of thermal energy in both the equilibration steps (adsorption and desorption) are the main contributions. These quantities decrease with the runs due to a reduced amount of $CO_2$ moving from bed to bed.

-Bed 5: this bed is always kept at 20°C. Cooling energy variation is related to the amount of $CO_2$ delivered from Bed 4 and decrease after run 3 as $CO_2$ begins to be stored also in the bulk gas phase.

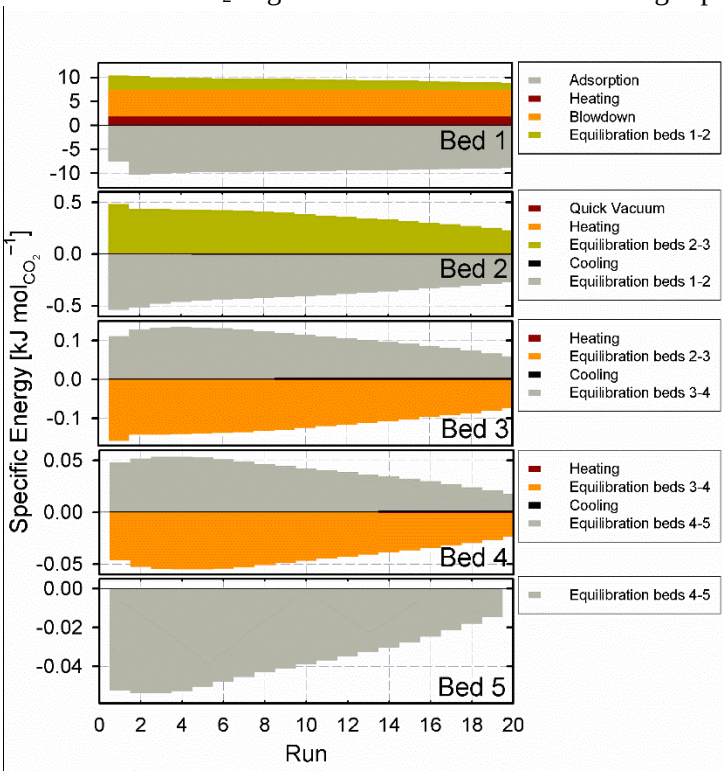


Figure 5: Specific energy (heating or cooling energy per mole of $CO_2$ captured in Bed 5) for the adsorbed phase state change in each bed of the system.

Table 7 reports the specific energy demand (energy per moles of $CO_2$ captured in Bed 5) due to the heat of adsorption and shows that Bed 1 contributes more than all the other beds to the energy consumption. As an aggregated index, summing up all bed masses, the heating energy for desorption is 180 $kJ_{th}$ $kg_{all\_beds}^{-1}$.

Table 7: Contribution of beds and compounds to the specific energy for adsorption (cooling) and desorption (heating) [$kJ_{th}$ $mol_{CO2inBed5}^{-1}$].

| | Specific energy of adsorption | |
|---|---|---|
| | Heating | Cooling |
| Bed 1 | 191 | –189 |
| Bed 2 | 7 | –8 |
| Bed 3 | 2 | –2 |
| Bed 4 | 1 | –1 |
| Bed 5 | 0 | 0 |

However, the highest contribution to the total specific energy demand consists of the sensible heat needed for each heating/cooling cycle of the solid adsorption material. Table 8 details how sensible heat is distributed in

the process. Heating of the solid sorbent accounts for 98% of the total sensible energy for heating and this amount of energy is required mainly in Bed 1. Therefore, a significant energy saving can be expected by application of heat recovery strategies and optimization of the heat transfer in Bed 1. This is usual in temperature swing adsorption processes [80, 81], arranging Bed 1 in low heat capacity-high thermal diffusivity structures is essential to contain the thermal energy losses and speed up process dynamics. The total specific sensible heat is 85% (1.78 $MJ_{th}$ $mol_{CO2}^{-1}$) of the total specific thermal energy consumed by the process for heating (2.08 $MJ_{th}$ $mol_{CO2}^{-1}$) at the operational conditions of Table 6. In addition, the total specific electrical energy consumption for the optional vacuum steps in Bed 1 and Bed 2 is 0.12 $MJ_{el}$ $mol_{CO2}^{-1}$ almost totally used in Bed 1 blowdown.

Table 8: Contribution of beds and gas mixture to the specific sensible heat [$MJ_{th}$ $mol_{CO2inBed5}^{-1}$].

| | Gas mixture | 13X solid sorbent | total | % sensible energy consumption |
|---|---|---|---|---|
| Bed 1 | 0.01 | 1.38 | 1.39 | 78% |
| Bed 2 | 0.01 | 0.25 | 0.26 | 15% |
| Bed 3 | 0.01 | 0.08 | 0.09 | 5% |
| Bed 4 | 0.01 | 0.03 | 0.04 | 2% |
| total | 0.04 | 1.74 | 1.78 | |
| % sensible energy consumption | 2% | 98% | | |

## 6. Process analysis

The analyses in the previous sections on a 5 beds process of given beds mass ratios (Table 6) are aimed at understanding the basic process operation. In general, number and masses of the beds must be adjusted to achieve a maximum in $CO_2$ purity in the storage bed at the minimum specific energy consumption. This leads to a multi-objective optimisation problem for the identification of the best trade-off curve (Pareto front) between these two objectives. Pareto fronts for 4, 5 and 6 beds processes using different materials are reported in Fig. 6 where the configuration described above is highlighted as base case in the wider ensemble of optimal configurations. The base case analysed in the previous sections is part of a family of configurations having different beds mass ratios, different storage bed mass and different specific amount of $CO_2$ stored [$mol_{CO2}$ $kg_{storage\ bed}^{-1}$].

Fig. 6 shows that the process can work also with 4 beds of zeolite 13X and only 10 runs but this will increase the energy needed to achieve $CO_2$ purities >0.95. An increase in the number of runs from 10 to 20 provides improved performance with higher purities achieved and lower energy required. A marginal advantage in purity can still be gained moving from 20 to 30 runs. In the region of interest (from Table 2 $CO_2$ purity >0.95 and energy <2.2 $MJ_{th}$ $mol_{CO2}^{-1}$) 4 beds and 5 beds processes perform identical to zeolite 13X.

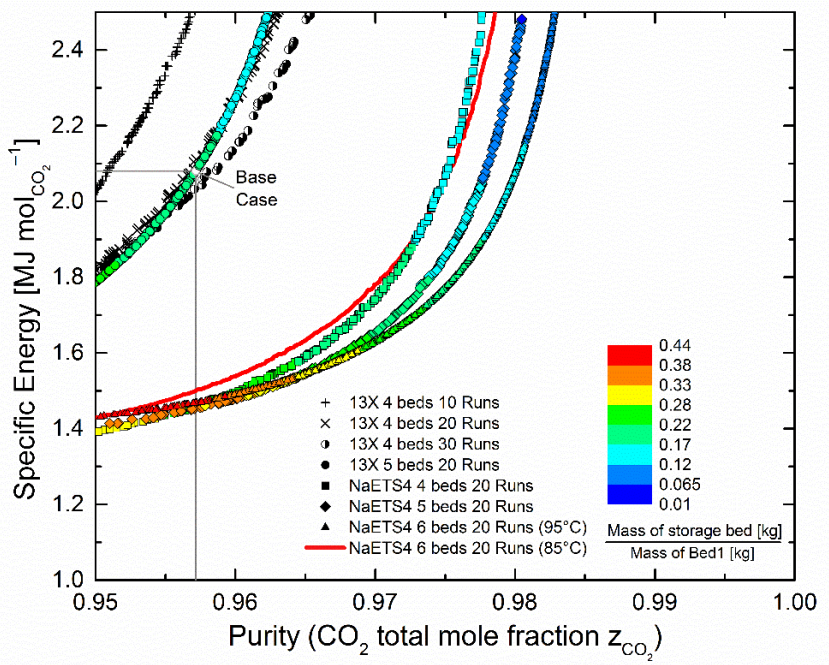


Figure 6: Pareto fronts for 4 and 5 beds processes of zeolite 13X, cycling for 10 to 30 runs. The base case highlighted is the previously analysed configuration of Table 6. The Pareto fronts of 4, 5 and 6 beds processes of zeolite NaETS-4 show a significant increase of the performance. The Pareto fronts of 6 beds process of NaETS-4 are shown at 95°C and 85°C regeneration temperature.

When zeolite NaETS-4 [66] is used a step-change in all the Pareto fronts is achieved at lower energy consumptions. At 2.2 $MJ_{th}$ $mol^{-1}$ $CO_2$ all the zeolite NaETS-4 Pareto fronts lie at $CO_2$ purities >0.97, perfectly matching the purity and energy specifications of Table 2. Zeolite NaETS-4 has unrivalled advantage due to its high selectivity value of ~2060 at atmospheric conditions, where extremely dilute $CO_2$ has to be adsorbed, compared to a selectivity of ~830 for zeolite 13X. This feature along with $\Delta H_{N2}$ lower than zeolite 13X leads to a lower amount of $N_2$ moving to the subsequent beds and the accomplishment of the purification with lower energy demand. When the process regeneration temperature is decreased to 85°C, the 6 beds process of NaETS-4 still performs within the purity and energy consumption requirements of Table 2, although the Pareto front is located at higher energy consumptions than the same process operating with regeneration temperature of 95°C. This is a direct result of a change of NaETS-4 selectivity at 85°C. Fig. 7 shows the recoveries that can be achieved by the process. In the region of interest, a 5 beds process of zeolite 13X achieves recoveries up to 42%, with a significant shift up to 60% when the process operates with zeolite NaETS-4.

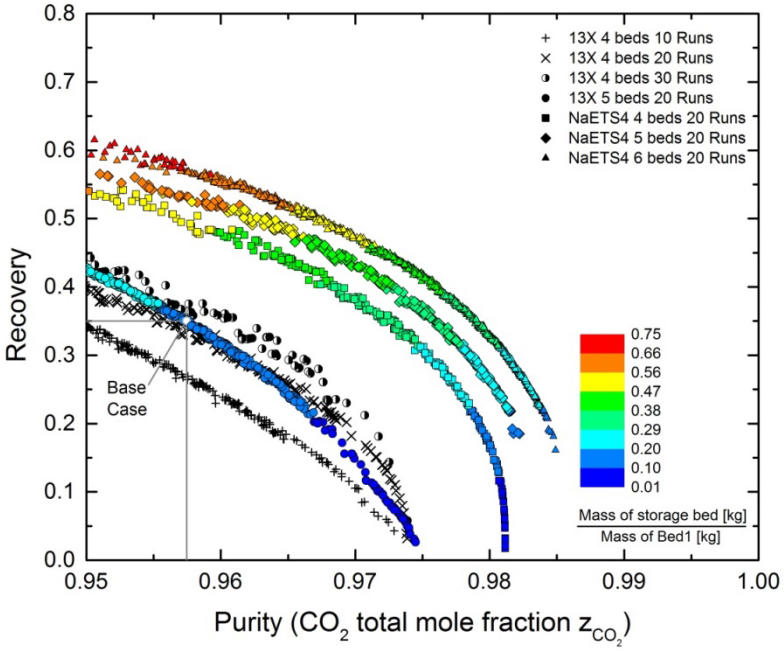


Figure 7: Recoveries for 4, 5 and 6 beds processes using zeolite 13X or zeolite NaETS-4 at 10, 20 and 30 Runs. Values are calculated subtracting the initial $CO_2$ already in the storage bed before Run 1.

## 7. Guidelines for shortcut process design

The purity achieved in the storage bed depends mainly on the specific amount adsorbed in the storage bed since the $CO_2$ contained in the bulk gas phase is negligible compared to the amount adsorbed. So, high purities can be achieved by using as storage materials those having high saturation capacity ($q_{s1} + q_{s2} = 5.64$ mol kg$^{-1}$ for zeolite 13X) and running the process until loadings close to the material saturation capacity are achieved. Fig. 8 shows that there is a correlation among specific amount of $CO_2$ loaded in the storage bed, purity and specific energy. It highlights that, in order to save energy, it is advisable to design the process for final $CO_2$ concentrations lower than the adsorption saturation value. This still allows to achieve $CO_2$ purities >0.95 mole fraction, to avoid too high specific energy consumptions and to know the mass of storage bed per mole of $CO_2$ stored.

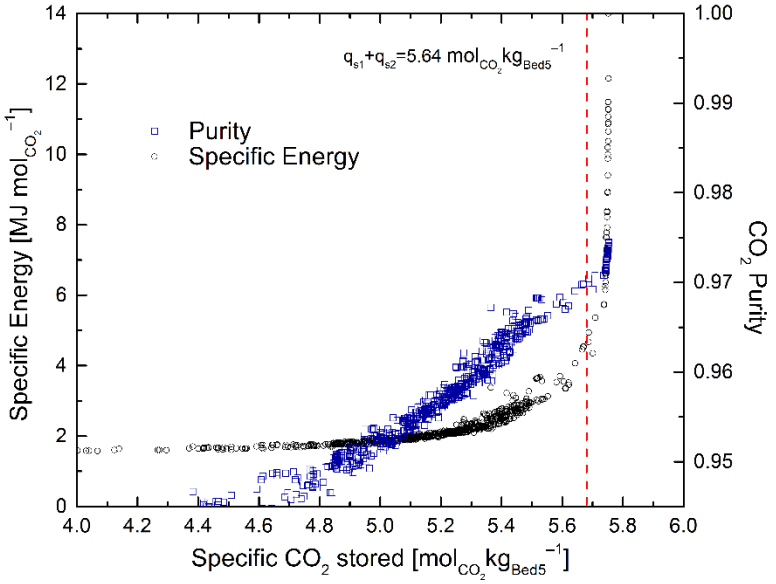


Figure 8: A design of the system aimed at loading Bed 5 at values below its saturation (5.64 mol$_{CO2}$ kg$^{-1}$ for zeolite 13X) leads to still high $CO_2$ purities and contained energy consumptions.

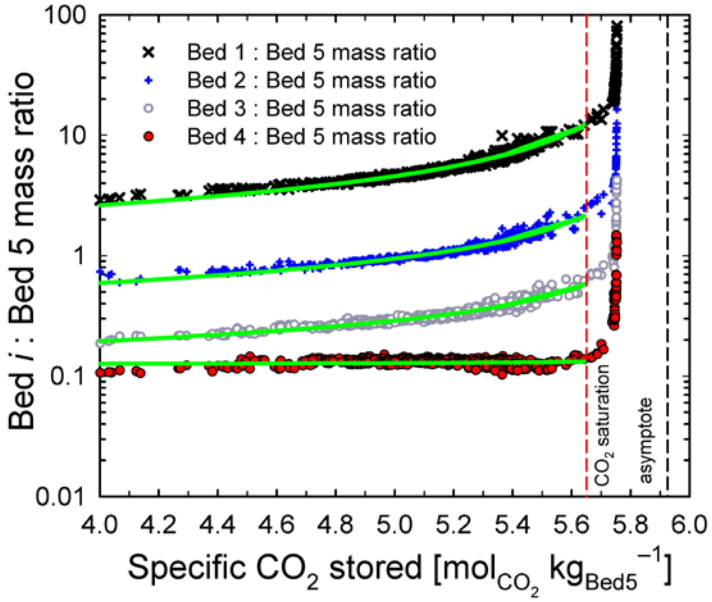


Figure 9: Correlation between specific $CO_2$ stored in Bed 5 and mass ratio *Bed j:Bed5* for the case of 5 beds process with zeolite 13X. Mass ratio depends on the design value chosen as specific $CO_2$ load in Bed 5 ($q_{load}$).

As illustrated in Fig. 6 and Fig. 9, a correlation exists between specific amount of $CO_2$ stored and Bed *j*:Bed 5 mass ratios. Furthermore, a regular pattern in *Bed j:Bed NB* mass ratios is present at low $CO_2$ loadings of Bed NB. In this region of interest, *Bed j:Bed NB* mass ratios follow the following six parameters empirical correlation:

$$\frac{mass\ Bed\ j}{mass\ storage\ bed} = \left[k + \left(a_{1,NB} - k\right) f^{-(j-1)}\right] + \left(c + \frac{b_{1,NB}}{j^{t\ NB}}\right) \frac{1}{\left(q_{asympt} - q_{load}\right)} \qquad \text{j=1,2,..NB} \qquad (18)$$

where $q_{asympt}$ [$mol_{CO2}\ kg^{-1}$] is the maximal amount of $CO_2$ stored in the storage bed (illustrated as asymptote in Fig. 9), $q_{load}$ [$mol_{CO2}\ kg^{-1}$] is the design value chosen as $CO_2$ loading for the storage bed (below the material saturation), NB is the total number of beds in the process and the vector of parameters ($a_{1,NB}$, $b_{1,NB}$, *f*, *k*, *c*, *t*) depends on the adsorption material and the total number of beds NB in the process. Table 9 include values of the vector ($a_{1,NB}$, $b_{1,NB}$, *f*, *k*, *c*, *t*) for zeolite 13X and zeolite NaETS-4. Eq. (18) is mainly affected by the parameters $a_{1,NB}$ and $b_{1,NB}$ which are assessed by considering only Bed 1 and Bed NB. Once this proportion is chosen, the beds of the compression train (from Bed *j+1* to Bed *NB–1*) follow reasonably well a geometric series of the form $(a_{1,NB} - k)\ f^{-(j-1)}$.

Table 9: Parameters of eq. (18)

| Process | Zeolite | $q_{asympt}$ [$mol_{CO2}\ kg^{-1}$] | $a_{1,NB}$ | $b_{1,NB}$ | f | k | c | t |
|---|---|---|---|---|---|---|---|---|
| 4 beds process | 13X | 5.406 | 0.184 | 2.000 | 0.680 | 0.0488 | –0.01222 | 0.6641 |
| | NaETS-4 | 3.864 | –0.199 | 1.291 | 1.807 | 0.8600 | –0.09005 | 3.0000 |
| 5 beds process | 13X | 5.864 | 0.104 | 3.692 | 0.674 | –0.0854 | –0.06800 | 0.5731 |
| | NaETS-4 | 3.864 | –0.199 | 1.287 | 1.787 | 0.6700 | –0.09015 | 1.1154 |
| 6 beds process | 13X | 5.864 | 0.120 | 4.360 | 1.040 | 0.0384 | –0.00395 | 0.4856 |
| | NaETS-4 | 3.903 | 0.067 | 1.513 | 1.420 | 0.0909 | –0.00289 | 0.5513 |

Note: eq. (18) can be used for the design of processes leading to a storage bed load below adsorption saturation

## 8. Conclusions

In order to provide a factual contribution to climate change mitigation a direct air capture technology must fulfil the strict requirements reported in Table 2 in terms of purity and pressure of the stored $CO_2$, energy consumption and capture rate. All the reviewed technological solutions for air capture fall short in one or more of these requirements, therefore needing of further research and development efforts. An alternative temperature swing adsorption process has been proposed and a thermodynamic analysis presented. The process consists of a series of adsorption beds powered by low grade heat. The thermodynamic analysis proves that the process is able to capture, purify and compress $CO_2$ extracted from an extremely dilute condition such as in the atmospheric air. Therefore, if coupled with renewable sources with a major contribution from solar thermal energy, the process is entirely carbon-negative, without generation of $CO_2$ at any point. When the process operates with 5 beds of zeolite 13X regenerated at 95°C and cooled at ambient temperature, $CO_2$ can be purified at values >0.95 mole fraction with a specific energy consumptions <2.2 $MJ_{th}\ mol_{CO2}^{-1}$, that are two of the features required to air capture. Advanced materials like zeolite NaETS-4 enable higher $CO_2$ purities at significantly lower energy consumption than zeolite 13X. The process is highly scalable by adjustment of the total amount of porous material loaded in each single bed. The present analysis identifies the ratios between two consecutive beds as the feature that most affects the performance. A straightforward shortcut correlation is provided to estimate the selection of mass ratios. Furthermore, the thermodynamic analysis presented enables the design of a practical unit, aimed at the investigation of the process dynamics to check how the process is able to meet the requirements on capture rate.

## 9. Acknowledgments

The research leading to these results has received funding from the European Union Seventh Framework Programme (FP7/2007-2013) under grant agreement n°630863.

**Nomenclature**

| | |
|---|---|
| $c_{p,ads}$ | Specific heat capacity of the adsorbent material [kJ $kg^{-1}$ $K^{-1}$] |
| $c_{p,i}$ | Specific heat capacity of component *i* [kJ $mol^{-1}$ $K^{-1}$] |
| f | Scaling factor for the masses of the beds; |
| F | Total number of moles in the feed [mol]; |
| G | Total number of moles in the bulk gas phase [mol]; |
| M | Total number of moles in the adsorbed phase [mol]; |
| $m_{ads}$ | Mass of adsorbent [kg]; |
| NB | Number of beds; |
| NC | Number of adsorbed components ($N_2$, $O_2$, $CO_2$); |
| $n_i$ | Specific amount adsorbed of component *i* [mol $kg^{-1}$] unless otherwise specified; |
| $n_{i,ads}$ | Amount of adsorbed moles of component *i* [mol] in adsorbed phase phase; |
| $n_{i,bulk}$ | Amount of adsorbed moles of component *i* [mol] in bulk gas phase; |
| $P_i^0$ | Surface pressure of the component *i* [kPa]; |
| $P_{bulk}$ | Pressure of the mixture in the bulk gas phase [kPa]; |
| $q_{load}$ | $CO_2$ design loading of the storage bed [$mol_{CO2}$ $kg^{-1}$]; |
| $q_{asympt}$ | Maximal asymptotic specific $CO_2$ that can be filled in the storage bed [$mol_{CO2}$ $kg^{-1}$]; |
| R | Universal gas constant [kJ $mol^{-1}$ $K^{-1}$]; |
| T | Equilibrium temperature [K]; |
| $T_{high}$ | Desorption temperature [K]; |
| $T_{low}$ | Adsorption temperature [K]; |
| $V_{void}$ | Volume occupied by the bulk gas phase [$m^3$]; |
| $W_{el}$ | Electrical energy for vacuum; |
| $x_i$ | Molar fraction of component *i* in the adsorbed phase; |
| $y_i$ | Molar fraction of component *i* in the bulk gas phase; |
| $z_i$ | Molar fraction of component *i* in the feed; |
| $\Delta H_{ads}$ | Enthalpy for adsorption or desorption [kJ]; |
| $\Delta H_{sens}$ | Sensible thermal energy [kJ]; |
| $\Delta \bar{h}_i$ | Differential enthalpy of adsorption [kJ $mol^{-1}$] for component *i* in the mixture; |
| $\Delta \bar{h}_i^0$ | Differential enthalpy of adsorption [kJ $mol^{-1}$] for pure component *i*; |
| $\Delta h_i^0$ | Integral enthalpy of adsorption [kJ $mol^{-1}$] for pure component *i*; |

**Subscripts**

| | |
|---|---|
| i | Component number in the gaseous mixture ($N_2$, $O_2$, $CO_2$); |
| j | Bed number; |

**Greek letters**

| | |
|---|---|
| $\varepsilon_b$ | Bed porosity; |
| $\varepsilon_p$ | Particle porosity; |
| $\rho_{bed}$ | Bed bulk density [kg $m^{-3}$]; |
| $\rho_{cr}$ | Crystal density [kg $m^{-3}$]; |
| $\psi_{eq}$ | Reduced grand potential at equilibrium [mol $kg^{-1}$]; |
| $\psi_i$ | Reduced grand potential of component *i* [mol $kg^{-1}$]; |

**References**


[1] N. Stern. Review Report on The Economics of Climate Change. (2006) HM Treasury, London.
[2] N. Stern. The criticality of the next 10 years, 28 October 2016, The Royal Society, London.
[3] Directive 2009/31/EC of the European Parliament and of the Council of 23 April 2009 on the geological storage of carbon dioxide and amending Council Directive 85/337/EEC.
[4] M. E. Boot-Handford, J. C. Abanades, E. J. Anthony, M. J. Blunt, S. Brandani, N. Mac Dowell et al. Carbon capture and storage update. *Energy Environ Sci*, 2014; **7**:130–89.
[5] A. Goeppert, M. Czaun, G. K. Surya Prakash, G. A. Olah. Air as the renewable carbon source of the future: an overview of $CO_2$ capture from the atmosphere. *Energy Environ Sci*, 2012; **5**:7833–53.
[6] IPCC 5th Assessment Report (2014). www.ipcc.ch.
[7] BP Statistical Review of World Energy 2016.
[8] F. Magnani, M. Mencuccini, M. Borghetti, P. Berbigier, F. Berninger, S. Delzon et al. The human footprint in the carbon cycle of temperate and boreal forests. *Nature* 2007;**447**:848–52.
[9] K. S. Lackner. The thermodynamics of direct air capture of carbon dioxide. *Energy* 2013;**50**:38–46.
[10] R. Zhao, S. Deng, Y. Liu, Q. Zhao, J.He, L. Zhao. Carbon pump: Fundamental theory and applications. *Energy* 2017;**119**:1131–43.
[11] D. M. Ruthven. $CO_2$ capture: Value functions, separative work and process economics. *Chem Eng Sci* 2014;**114**:128-33.
[12] D. M. Ruthven, S. Farooq, S. Brandani. Work of separation in $CO_2$ capture: Applicability of the value function. *Chem Eng Sci* 2015;**126**:604–7.
[13] S. Brandani. Carbon dioxide capture from air: a simple analysis. *Energy Environ* 2012;**23**:319-32.
[14] NASA Surface meteorology and Solar Energy. A renewable energy resource web sitehttps://eosweb.larc.nasa.gov/cgi-bin/sse/sse.cgi?skip@larc.nasa.gov+s02#s02
[15] G. Santori, A. Sapienza, A. Freni. A dynamic multi-level model for adsorptive solar cooling. *Renew Energy* 2012;**43**:301-12.
[16] J.A. Duffie, W.A. Beckmann. Solar engineering of thermal processes, 4th edition, John Wiley and sons, 2013, Hoboken, New Jersey.
[17] K. Johnsen, K. Helle, T. Myhrvold. Scale-up of $CO_2$ capture processes: The role of Technology Qualification. *Energy Proc* 2009;**1**:163–70.
[18] J. Harmsen. Industrial Process Scale-up: A Practical Guide from Idea to Commercial Implementation. The Boulevard, Langford Lane, Kidlington, Oxford, OX5 1GB, UK, Elsevier.
[19] P. Smith, R. S. Haszeldine, S. M. Smith. Preliminary assessment of the potential for, and limitations to, terrestrial negative emission technologies in the UK. *Environ Sci: Process & Impacts* 2016;**18**:1400–5.
[20] K. Z. House, A. C. Baclig, M. Ranjan, E. A. van Nierop, J. Wilcox, H, J. Herzog. Economic and energetic analysis of capturing $CO_2$ from ambient air. *PNAS* 2011;**108**:20428–33.
[21] C. Pritchard, A. Yang, P. Holmes, M. Wilkinson. Thermodynamics, economics and systems thinking: What role for air capture of $CO_2$?. *Process Saf Environ* 2015;**94**:188–95.
[22] M. M. Lozinska, E. Mangano, J. P. S. Mowat, A. M. Shepherd, R. F. Howe, S. P. Thompson et al. Understanding Carbon Dioxide Adsorption on Univalent Cation Forms of the Flexible Zeolite Rho at Conditions Relevant to Carbon Capture from Flue Gases. *JACS* 2012;**134**:17628–42.
[23] Y. Wang, D. LeVan. Adsorption Equilibrium of Binary Mixtures of Carbon Dioxide and Water Vapor on Zeolites 5A and 13X. *J Chem Eng Data* 2010;**54**:3189-95.
[24] E. S. Sanz-Perez, C. R. Murdock, S. A. Didas, C. W. Jones. Direct capture of $CO_2$ from ambient air. *Chem Rev* 2016;**116**:11840–76.
[25] J. V. Veselovskaya, V. S. Derevschikov, T. Y. Kardash, O. A. Stonkus, T. A. Trubitsina, A. G. Okunev. Direct $CO_2$ capture from ambient air using $K_2CO_3/Al_2O_3$ composite sorbent. *Int J Greenh Gas Con* 2013;**17**:332–40.
[26] V. S. Derevschikov, J. V. Veselovskaya, T. Y. Kardash, D. A. Trubitsyn, A. G. Okunev. Direct $CO_2$ capture from ambient air using $K_2CO_3/Y_2O_3$ composite sorbent. *Fuel* 2014;**127**:212–8.
[27] M. Varghese, L. Mulloth, B. Luna, J. Hogan. Development status of a Low-Power $CO_2$ Removal and Compression System for Closed-Loop Air Revitalization, 40th International Conference on Environmental Systems. https://doi.org/10.2514/6.2010-6060
[28] S. U. Rege, R. T. Yang, M. A. Buzanowski. Sorbents for air prepurification in air separation. *Chem Eng Sci* 2000;**55**:4827–38.

[29] P. Markewitz, W. Kuckshinrichs, W. Leitner, J. Linssen, P. Zapp, R. Bongartz et al. Worldwide innovations in the development of carbon capture technologies and the utilization of $CO_2$. *Energy Environ Sci* 2012;**5**:7281-305.
[30] E. de Visser, C. Hendriks, M. Barrio, M. J. Mølnvik, G. de Koeijer, S. Liljemark et al. Dynamis $CO_2$ quality recommendations. *Int J Greenh Gas Con* 2008;**2**:478–84.
[31] E. Goos, U. Riedel, L. Zhao, L. Blum. Phase diagrams of $CO_2$ and $CO_2$-$N_2$ gas mixtures and their application in compression processes. *Energy Proc* 2011;**4**:3778–85.
[32] M. Mazzoccoli, B. Bosio, A. Arato, S. Brandani. Comparison of equations-of-state with P-ρ-T experimental data of binary mixtures rich in $CO_2$ under the conditions of pipeline transport. *J Supercr Fluids* 2014;**95**:474–90.
[33] K.S. Lackner. Climate change. A guide to $CO_2$ sequestration. *Science*, 2003;**300**, 1677-78.
[34] D. W. Keith, M. Ha-Duong, J. Stolaroff, Climate Strategy with $CO_2$ Capture from the Air. *Clim Change* 2006;**74**:17–45.
[35] F. Zeman. Energy and Material Balance of $CO_2$ Capture from Ambient Air. *Environ Sci Technol* 2007;**41**:7558–63.
[36] R. Baciocchi, G. Storti, M. Mazzotti. Process Design and Energy Requirements for the Capture of Carbon Dioxide from Air. *Chem Eng Process: Process Intensif* 2006;**45**:1047–58.
[37] V. Nikulshina, C. Gebald, A. Steinfeld. $CO_2$ capture from atmospheric air via consecutive CaO-carbonation and $CaCO_3$-calcination. *Chem Eng J* 2009;**146**:244–48.
[38] M. Mahmoudkhani, D. W. Keith. Low-energy sodium hydroxide recovery for $CO_2$ capture from atmospheric air—Thermodynamic analysis. *Int J Greenh Gas Con* 2009;**3**:376–84.
[39] K. S. Lackner. Capture of carbon dioxide from ambient air. *Eur Phys J Special Topics* 2009;**176**:93–106.
[40] K. S Lackner. Washing Carbon Out of the Air. *Sci Am* 2010;**302**:66–71.
[41] T. Wang, K. S. Lackner, A. Wright. Moisture swing sorbent for carbon dioxide capture from ambient air. *Environ Sci Technol* 2011;**45**:6670–75.
[42] D. S. Goldberg, K. S. Lackner, P. Han, Al. L. Slangle, T. Wang. Co-location of air capture, subseafloor $CO_2$, sequestration, energy production on Kerguelen Plateau. *Env Sci Technol* 2013;**47**:7521–29.
[43] R. A. Kulkarni, D. S. Sholl. Analysis of Equilibrium-Based TSA Processes for Direct Capture of $CO_2$ from Air. *Ind Eng Chem Res* 2012;**51**:8631−45.
[44] W. Zhang, H. Liu, C. Sun, T. P. Drage, C. E. Snape. Capturing $CO_2$ from ambient air using polyethyleneamine-silica adsorbent in fluidized beds. *Chem Eng Sci* 2014;**116**:306–16.
[45] S.A. Kalogirou. Solar thermal collectors and applications. *Prog Energy Combust Sci* 2004;**30**:231–95.
[46] J. A. Wurzbacher, C. Gebald, A. Steinfeld. Separation of $CO_2$ from air by temperature-vacuum swing adsorption using diamine-functionalized silica gel. *Energy Environ Sci* 2011;**4**:3584–92.
[47] J. A. Wurzbacher, C. Gebald. Patent Number WO2013075981;
[48] P. A. Webley, Adsorption technology for $CO_2$ separation and capture: a perspective. *Adsorption* 2014;**20**:225–31.
[49] J. A. Wurzbacher, C. Gebald, S. Brunner, A. Steinfeld. Heat and mass transfer of temperature–vacuum swing desorption for $CO_2$ capture from air. *Chem Eng J* 2016;**283**:1329–38.
[50] S. L'Orange Seigo, S. Dohle, M. Siegrist. Public perception of carbon capture and storage (CCS): A review. *Renew Sust Energy Rev* 2014;**38**:848–63.
[51] C. Sun, X. Yuan, X. Yao. Social acceptance towards the air pollution in China: Evidence from public's willingness to pay for smog mitigation. *Energy Policy* 2016;**92**:313–24.
[52] A. Marcussi, S. Kypreos, E. Panos. The road to achieving the long-term Paris targets: energy transition and the role of direct air capture. *Clim Change* 2017;**144**:181–93.
[53] IEA-SHC Task 48 “Quality Assurance & Support Measures for Solar Cooling Systems”, http://task48.iea-shc.org
[54] S. Sircar. Pressure Swing Adsorption Technology. Volume 158 (1989) of the series NATO ASI Series 285-321 in Adsorption: Science and Technology Part III Ed. A.E. Rodrigues, M.D. LeVan, D. Tondeur. Springer.
[55] F. Rezaei, P. Webley. Optimum structured adsorbents for gas separation processes. *Chem Eng Sci* 2009;**64**:5182—91.
[56] A. Freni, L. Bonaccorsi, L. Calabrese, A. Caprì, A. Frazzica, A. Sapienza. SAPO-34 coated adsorbent heat exchanger for adsorption chillers. *Appl Therm Eng* 2015;**82**:1–7.
[57] D. M. Ruthven, C. Thaeron. Performance of a Parallel Passage Adsorbent Contactor. *Gas Sep Purif* 1997;**12**, 43-60.

[58] F. Rezaei, P. Webley. Structured adsorbents in gas separation processes. *Sep Pur Technol* 2010;**70**:243–56.
[59] R. P. Hoover, P. C. Wankat. Gas compression using temperature swing adsorption. *Sep Sci Technol* 2002;**37**:3187–99.
[60] G. Santori, M. Luberti. Thermodynamics of thermally-driven adsorption compression. *Sust Mat Technol* 2016;**10**:1–9.
[61] M.C. Ferrari, D. Friederich, G. Santori, S. Brandani. Design of a small scale air capture system, 11th International Conference on the Fundamentals of Adsorption, 19-24 May 2013, Baltimore (USA).
[62] R. Kumar. Adsorption Column Blowdown: Adiabatic Equilibrium Model for Bulk Binary Gas Mixtures. *Ind Eng Chem Res*, 1989;**28**:1677–83.
[63] C. Charalambous, G. Santori, E. Vilarrasa-Garcia, M. Bastos-Neto, C. L. Cavalcante, S. Brandani. Pure and Binary Adsorption of Carbon Dioxide and Nitrogen on AQSOA FAM Z02. *J Chem Eng Data* 2018;**63**:661–70.
[64] M. J. Goldsworthy. Measurements of water vapour sorption isotherms for RD silica gel, AQSOA-Z01, AQSOA-Z02, AQSOA-Z05 and CECA zeolite 3A. *Microporous Mesoporous Mater* 2014;**196**:59–67.
[65] M. L. Zanota, N. Heymans, F. Gilles, B. L. Su, M. Frère, G. De Weireld. Adsorption Isotherms of Pure Gas and Binary Mixtures of Air Compounds on Faujasite Zeolite Adsorbents: Effect of Compensation Cation. *J Chem Eng Data* 2010;**55**:448–58.
[66] R.S. Pillai, S.A. Peter, R.V. Jasra. Adsorption of carbon dioxide, methane, nitrogen, oxygen and argon in NaETS-4. *Microporous Mesoporous Mater* 2008;**113**:68–76.
[67] A. L. Myers, J. M. Prausnitz. Thermodynamics of mixed-gas adsorption. *AIChE J* 1965;**11**:121–7.
[68] K. S. Walton, D. S. Sholl. Predicting multicomponent adsorption: 50 years of the ideal adsorbed solution theory. *AIChE J* 2015;**91**:2757–62.
[69] J. A. O'Brien, A. L. Myers. A comprehensive technique for equilibrium calculations in adsorbed mixtures: the generalized FastIAS method. *Ind Eng Chem Res* 1988;**27**:2085–92.
[70] E. Mangano, D. Friedrich, S. Brandani. Robust algorithms for the solution of the ideal adsorbed solution theory equations. *AIChE J* 2015;**61**:981–91.
[71] G. Santori, M. Luberti, H. Ahn. Ideal adsorbed solution theory solved with direct search minimisation. *Comput Chem Eng* 2014;**71**:235–40.
[72] H. Davarzani, M. Marcoux, P. Costeseque, M. Quintard. Experimental measurement of the effective diffusion and thermodiffusion coefficients for binary gas mixture in porous media. *Chem Eng Sci* 2010;**65**:5092–104.
[73] Y. Demirel. Nonequilibrium Thermodynamics: Transport and Rate Processes in Physical, Chemical and Biological Systems (Second Edition), University of Nebraska, Lincoln, USA.
[74] A. Myers, P.A. Monson. Physical adsorption of gases: the case for absolute adsorption as basis for thermodynamic analysis. *Adsorption* 2014;**20**:591–622.
[75] K.S. Walton, M. D. LeVan. Adsorbed-Phase Heat Capacities: Thermodynamically Consistent Values Determined from Temperature-Dependent Equilibrium Models. *Ind Eng Chem Res* 2005;**44**:178–182.
[76] X. Hu, E. Mangano, D. Friedrich, H. Ahn, S. Brandani. Diffusion mechanism of $CO_2$ in 13X zeolite beads. *Adsorption* 2014;**20**:121-35.
[77] G. D. Oreggioni, S. Brandani, M. Luberti, Y. Baykan, D. Friedrich, H. Ahn. $CO_2$ capture from syngas by an adsorption process at a biomass gasification CHP plant: its comparison with amine-based $CO_2$ capture. *Int J Greenh Gas Con* 2015;**35**:71–81
[78] E.W. Lemmon, M.O. McLinden, M.L. Huber. NIST Standard Reference Database 23, NIST Thermodynamic Properties of Refrigerants and Refrigerant Mixtures Database (REFPROP) Version 9.0, Gaithersburg: National Institute of Standards and Technology (2010).
[79] G. Santori, A. Frazzica, A. Freni, M. Galieni, L. Bonaccorsi, F. Polonara et al. Optimization and testing on an adsorption dishwasher. *Energy* 2013;**50**:170–6.
[80] V. Palomba, S. Vasta, G. Giacoppo, L. Calabrese, G. Gulli, D. La Rosa et al. Design of an innovative graphite heat exchanger for adsorption heat pumps and chillers. *Energy Proc* 2015;**81**:1030–40.
[81] L. W. Wang, S. J. Metcalf, R. E. Critoph, Z. Tamainot-Telto, R. Thorpe. Two types of natural graphite host matrix for composite activated carbon adsorbents. *Appl Therm Eng* 2013;**50**:1652–7.